

# Hyperosmolarity-induced lipid droplet formation depends on ceramide production by neutral sphingomyelinase 2<sup>S</sup>

Alexandra Robciuc,<sup>\*,†</sup> Tuulia Hyötyläinen,<sup>§</sup> Matti Jauhiainen,<sup>†</sup> and Juha M. Holopainen<sup>1,\*</sup>

Helsinki Eye Lab,\* Department of Ophthalmology, Haartmaninkatu 4 C, University of Helsinki, 00290 Helsinki, Finland; Public Health Genomic Unit,<sup>†</sup> National Institute for Health and Welfare, Helsinki, Finland; and VTT Technical Research Centre of Finland,<sup>§</sup> Espoo, Finland

**Abstract** Hyperosmolarity (HO) imposes a remarkable stress on membranes, especially in tissues in direct contact with the external environment. Our efforts were focused on revealing stress-induced lipid changes that precede the inflammatory cytokine response in human corneal epithelial cells exposed to increasing osmolarity. We used a lipidomic analysis that detected significant and systematic changes in the lipid profile, highly correlated with sodium concentrations in the medium. Ceramides and triglycerides (TGs) were the most-responsive lipid classes, with gradual increases of up to 2- and 3-fold, respectively, when compared with control. The source of ceramide proved to be sphingomyelin hydrolysis, and neutral sphingomyelinase 2 (NSM2) activity showed a 2-fold increase 1 h after HO stress, whereas transcription increased 3-fold. Both TG accumulation and IL-8 secretion were shown to be dependent on ceramide production by specific knock-down of NSM2. In HCE cells, diglyceride acyltransferase 1 was responsible for the TG synthesis, but the enzyme activity had no effect on cytokine secretion. Hence, NSM2 plays a key role in the cellular response to hyperosmolar stress, and its activity regulates both cytokine secretion and lipid droplet formation.—Robciuc, A., T. Hyötyläinen, M. Jauhiainen, and J. M. Holopainen. Hyperosmolarity-induced lipid droplet formation depends on ceramide production by neutral sphingomyelinase 2. *J. Lipid Res.* 2012. 53: 2286–2295.

**Supplementary key words** liquid chromatography-mass spectrometry • cornea • proinflammatory cytokines

Hyperosmolarity (HO) imposes a remarkable stress on membranes. HO affects cellular balance and the changes in cell volume require membrane reorganization (1). Most affected tissues are those in direct contact with the external environment and are constantly exposed to variations in

osmolar pressure. One such site is the corneal epithelium, and disturbances in tear film composition and volume are causes for dry eye syndrome (DES), the most-common ocular pathology among people seeking eye care (2). DES, as an HO-induced inflammatory disease, is characterized by eye irritation symptoms, blurred and fluctuating vision, tear film instability, increased tear osmolarity, and ocular surface epithelial disease (3). Most of its manifestations are caused by the stress response of the corneal epithelial cells.

The sphingomyelin (SM) pathway was shown to be engaged in the response to numerous stress agents (ultraviolet radiation, lipopolysaccharide, serum deprivation) and provides fast and intensity-modulated defensive feedback (4–6). It consists of a cascade of reactions centered on SM hydrolysis to ceramide by specific enzymes, sphingomyelinases. Altered levels of the different sphingolipid species can have profound consequences on cell phenotype, and indeed, the balance of interdependent sphingolipids produced in the cell membrane can predict cellular behavior (7). Due to its organization, the SM pathway provides decision points in the cell's stress survival process and has therefore remained an evolutionarily preferred signaling system.

Another cellular stress response that has become widely studied in recent years is lipid droplet (LD) formation (for comprehensive review, see Refs. 8, 9). All cells, eukaryotes as well as prokaryotes (10), have the machinery needed

Abbreviations: ASM, acid sphingomyelinase; ATGL, adipose tissue triglyceride lipase; BEL, bromoenol lactone; Cer, ceramide; DES, dry eye syndrome; DGAT1,2, diglyceride acyltransferase 1,2; HCE, human corneal epithelial cells; HO, hyperosmolarity; LD, lipid droplet; PLA2, phospholipase A2; NSM, neutral sphingomyelinase; PE, phosphatidylethanolamine; SIP, sphingosine-1-phosphate; Sph, sphingosine; TG, triglyceride.

<sup>1</sup>To whom correspondence should be addressed.

e-mail: juha.holopainen@hus.fi.

<sup>S</sup>The online version of this article (available at <http://www.jlr.org>) contains supplementary data in the form of one table and four figures.

Copyright © 2012 by the American Society for Biochemistry and Molecular Biology, Inc.

This article is available online at <http://www.jlr.org>

This work was supported by grants from the Sigrid Juselius Foundation (J.M.H.), the Finnish Academy, Grant 132 629 (M.J.) and Grant 128 128 (J.M.H.), the Helsinki University Central Hospital Research Foundation (J.M.H.), and the Finnish Eye Foundation (J.M.H.).

Manuscript received 7 August 2012 and in revised form 15 August 2012.

Published, JLR Papers in Press, August 15, 2012

DOI 10.1194/jlr.M026732

for LD formation, and the recent focus on their structure has led to a broader view of their roles in cell physiology. LDs do not emerge only from a cell's need to store FAs or sterols. Under stress conditions, their formation is induced even in the absence of an extracellular source of lipids. Many environmental challenges, such as cell crowding, apoptosis, or the inflammatory response, have been described to induce neutral lipid accumulation (11–13). The cellular function of LDs is considered both detrimental as well as protective. The first is illustrated by eicosanoids production from the FFAs released during triglyceride (TG) hydrolysis (14), whereas the protective effect was hinted at by longer survival under stress of cells that produce TGs (15). Membrane phospholipids provide the building blocks for stress-induced LD synthesis (16).

In the present study, we aimed to assess adjustments in the lipid profile of HO-stressed cells and to identify the most-dynamic lipid species as well as the key modulators of this stress response. For these purposes, we used a corneal epithelial cell line (HCE2) to illustrate that HO induces remarkable changes in cellular lipid homeostasis and that the sphingolipid signaling pathway plays an important role in the response to this external stimulus. SM hydrolysis is an early event in HO stimulation, and the stress-induced enzyme in the sphingomyelinase pathway is neutral sphingomyelinase 2 (NSM2). Furthermore, HO-induced stress droplet formation, as well as IL-8 secretion, is an event controlled by the same enzymes, and this outcome may be relevant in the clinical context.

## MATERIALS AND METHODS

### Cells

Human corneal epithelial cells (HCEs) were grown and maintained in DMEM/F12 with 15% FBS and 10 ng/ml epithelial growth factor, 5 µg/ml insulin, 1 µg/ml l-glutamine, 40 µg/ml gentamicin (all supplied by Invitrogen; Carlsbad, CA), and 0.1 µg/ml cholera toxin (Sigma; St. Louis, MO) at 37°C under 5% CO<sub>2</sub> in a humidified incubator (17). Cells were subcultured every 3 days for 10–15 passages after defrosting and serum-starved for 18 h before experiments. Standard growth medium contained 140 mM NaCl and had an osmolality of 317 mOsm/kg. The osmolality of the media was increased by adding 5 M NaCl solution. Therefore, the molar concentrations specified in RESULTS, in the range of 50 to 140 mM, represent the added NaCl concentrations above the fixed salt content of the growth medium. For transfection, cells were subcultured in antibiotic-free medium at preconfluence density and transfected on the following day.

### Lipid extraction and nontargeted lipidomic analysis

Lipids were extracted from cell suspension using the Bligh-Dyer protocol (18). Briefly, the cells were grown on 6-well plates, washed with cold PBS, and scraped in 0.9 ml of 2% NaCl solution. An aliquot of 0.1 ml was used for protein concentration measurements, whereas the remaining 0.8 ml was mixed with chloroform and methanol (0.8:1:2, v/v), and the sample was centrifuged to eliminate debris. Next, for the phase separation, 1 ml water and 1 ml chloroform were added and the samples centrifuged. The lower phase was aspirated to a clean glass tube, and solvents were evaporated under nitrogen. Samples were stored at –20°C until analysis. The cell extracts were analyzed on an

Acquity Ultra Performance liquid chromatograph combined with a Waters Q-ToF Premier mass spectrometer (19). The column (at 50°C) was an Acquity UPLCTM BEH C18, 2.1 × 100 mm with 1.7 µm particles. The solvent system included ultrapure water (1% 1 M NH<sub>4</sub>Ac, 0.1% HCOOH) (A) and (B) LC/MS-grade acetonitrile/isopropanol (1:1, 1% 1M NH<sub>4</sub>Ac, 0.1% HCOOH). The gradient started from 65% A/35% B, reached 80% B in 2 min, and 100% B in 7 min, and remained there for 7 min. The flow rate was 0.4 ml/min, and the injected amount was 2.0 µl. The lipid profiling was carried out using ESI in positive mode, and the data were collected at a mass range of *m/z* 300–1,200. The data were processed using MZmine2 software (20). Lipids were identified using an internal spectral library. The data were normalized using internal standards representatives of each class of lipid present in the samples [PC(17:0/0:0), PC(17:0/17:0), PE(17:0/17:0), Cer(d18:1/17:0), and TG(17:0/17:0/17:0)]. Finally, the data were further normalized by dividing the normalized lipid concentration with the protein content of the sample. The differences between samples were compared using Student's *t*-test. To account for the multiple testing issues, *q* values indicating the false discovery rate were calculated. Median values of the lipids were used for calculating fold changes, and if the fold change was <1, the inverse negative of the value was taken. The heat map showing the fold changes was constructed by taking the median value of each group and comparing it to the median value of control samples. Correlation between lipid concentrations and added concentration of NaCl was calculated using Pearson's correlation.

Sphingomyelinase activity was measured using the AmplexRed sphingomyelinase assay kit (Invitrogen) under both neutral as well as acidic conditions as recommended by the manufacturer. Cells grown on 6 cm plates were washed and scraped in PBS on ice. The cells were then pelleted by centrifugation at 400 *g* for 10 min at 40°C and resuspended in distilled water. The whole-cell lysate was prepared by sonication of the cell suspension in water for 10 s using a Soniprep 150 (SanyoElectric; Tokyo, Japan). A 1:10 (v/v) dilution of the lysate in sodium acetate buffer (pH 5.0) was used for acid sphingomyelinase activity measurement, whereas for neutral sphingomyelinases, the sample was diluted 1:5 (v/v) in 0.1 M Tris-HCl, 10 mM MgCl<sub>2</sub> (pH 7.4). Reaction mixtures were incubated in the dark at 37°C for 30 to 60 min. Fluorescence was measured with Victor 2 Multilabel Counter (Wallac; Turku, Finland) with excitation at 535 nm and emission at 585 nm. Standard curves were prepared for each reaction, from the positive-control enzyme provided with the kit. Results were normalized to protein concentration and experimental control and presented as fold change.

### Gene expression analysis

Total RNA was extracted using the RNeasy Mini Kit (QIAGEN; Hilden, Germany), and 1 µg was converted into cDNA utilizing a first-strand synthesis kit (Fermentas; St. Leon-Rot, Germany) and following the protocol recommended by the manufacturer. Subsequently, 50 ng cDNA were used per reaction in Q-PCR with SYBR Green/ROX FastStart Universal master mix (Roche; Basel, Switzerland). The reaction was performed in 25 µl final volume and 0.2 µM of each primer in an ABI Prism7000 thermo cycler (Life Technologies Corporation; Carlsbad, CA). The sequence for used primers is given in supplementary Table I. As control gene, we have used human actin, and expression was quantified by calculating ddCt and 2-ddCt, graphically represented as fold change.

Sphingosine-1-phosphate (S1P) production was quantified abiding by a protocol previously published (21). Cells readily take up the [3H]sphingosine (Perkin Elmer; Waltham, MA) and then convert it intracellularly to [3H]S1P and further metabolites.

For these measurements, HCEs were cultured on 6-well plates; and after experiments, media was collected, cleared of cells and debris by centrifugation, and mixed with equal volumes of methanol, chloroform, and 0.1 N NaOH. After the phase separation, under alkaline solvent extraction conditions, SIP is negatively charged and partitions into the aqueous phase, whereas other neutral sphingolipids, including sphingosine, are retained in the organic phase. In this manner we could measure both secreted as well as intracellular SIP. For intracellular SIP levels, cells were collected in 1 M NaCl. A small part was saved for protein analysis, whereas the remainder was used for lipid extraction, similarly to the conditioned medium. Counts per minute were then normalized to protein concentration.

### Oil Red O staining fluorescence microscopy and quantification

Cells grown on glass coverslips were used for Oil Red O fluorescence microscopy. After the media was removed, the cells were carefully washed with PBS and fixed with 10% formalin in PBS. Oil Red O staining solution was freshly prepared by mixing 3% Oil Red O solution in isopropanol with water (3:2, v/v), and cells were stained for 5 min and then rinsed with water. Samples were visualized on an Axioplan 2 fluorescence microscope (Carl Zeiss, AG; Germany) with a Plan Neofluar 40 $\times$ /0.75 (DIC II) air objective. Images were acquired at room temperature with an AxioCamHR camera. For quantitative data, cells grown in 12-well plates were stained with Oil Red O as described above. After rinsing, the retained Oil Red O dye was extracted with 300  $\mu$ l of 100% isopropanol, and 250  $\mu$ l were pipetted into 96-well plates for absorbance measurement at 490 nm (Wallac Victor 2 Multilabel Counter; Turku, Finland). As blank, we used similarly processed cell-free wells. Data are presented as absorbance at 490 nm of samples after blank subtraction.

### Lipolysis assay

To measure TG hydrolysis, we used a previously described radiometric method (22). Cells were cultured on 10 cm-diameter plates, washed, and scraped in PBS. Cells were pelleted and lysed by brief sonication in the assay buffer (0.2 M Tris-HCl buffer, pH 8.4, with 0.1 M NaCl). The lipolytic activity of 0.2 ml of cellular lysate was measured using labeled triolein (30 nmol/assay). The reaction mixture was incubated for 60 min at 37°C and terminated by adding 3.25 ml of methanol-chloroform-heptane (10:9:7, v/v) and 1 ml of 0.14 M potassium carbonate-0.14 M boric acid, pH 10.5. The samples were then centrifuged (1,600 *g* for 15 min), and the radioactivity in 1 ml of the upper phase was determined by liquid scintillation counting. Results were normalized to protein concentration.

### IL-8 ELISA

For IL-8 secretion analysis, a commercial ELISA DuoSet kit (R and D Systems; Minneapolis, MN) was used. The assay plates were prepared as recommended by the manufacturer. Media was collected from culture plates and centrifuged for 10 min at 400 *g* to eliminate floating cells and debris and stored frozen until measured. For assays, 60  $\mu$ l of media were mixed with an equal volume of reagent diluent, and 100  $\mu$ l were pipetted onto the plates coated with the capture antibody. Plates were analyzed using the microplate reader Victor 2 Multilabel Counter (Wallac) at a wavelength of 450 nm. To calculate the concentration, the standards were fitted with a second-order polynomial equation. Concentrations were reported as pg/ml.

### Cytokine secretion

For parallel determination of relative levels of secreted cytokines and chemokines, we have used a proteome profiler array (Human Cytokine Array Panel A, R and D Systems; Minneapolis,

MN). The array measured concomitantly the levels of 36 different cytokines and chemokines (spotted in duplicates on a nitrocellulose paper). Samples were prepared following the manufacturer's instructions. Briefly, conditioned media from confluent cells was cleared of floating cells and debris and an aliquot of 700  $\mu$ l was mixed with the kit reagents and assayed immediately.

### siRNA transfection

We used DharmaFECT SMART pool, a mixture of four short, interfering RNAs (siRNAs) targeting the human NSM2 gene (accession number NM\_018667.3) (Dharmacon; Lafayette, CO). Cells were transfected at 70% confluence in 12-well plates by adding to each well 25 pmol of the siRNA pool and 3  $\mu$ l of Dharmafect Transfection Reagent 1. The transfection protocol followed the manufacturer's instructions. Before experiments, cells were serum-starved overnight at 36 h after the transfection. As control for transfection experiments, we used nontargeting siRNA.

### Statistical analysis

Statistical analysis was performed using GraphPad Prism 4.03 (GraphPad Software, Inc.; La Jolla, CA). Statistical significance was determined by *t*-test or ANOVA on values from an average of three independent experiments. Data are reported as mean  $\pm$  SEM unless otherwise specified. Values of *P* < 0.05 were considered significant.

## RESULTS

Osmotic stress has been associated with inflammation for almost a decade, and most of its organ-level effects are a consequence of increased secretion of proinflammatory molecules (23). Therefore, we measured HO-induced cytokine secretion by corneal epithelial cells using a protein array (Fig. 1A). As control, we used cells incubated in normosmolar medium (317 mOsm/kg with 140 mM NaCl). The osmolarity of the media was increased by addition of 5 M NaCl to reach the specified molar concentrations. The pro-inflammatory cytokines found to be modulated by HO in HCE cells (IL-8, IL-6, MIF, and GRO $\alpha$ ) have been previously observed in tears of patients with inflammatory eye diseases (24, 25).

Because IL-8 is regarded as an acute-phase chemokine and has proved to be highly modulated by osmolarity, we used ELISA to determine the time course of the cytokine response (Fig. 1B). A significant increase in IL-8 secretion was evident 3 to 4 h after the stress induction.

We next intended to distinguish early lipid alterations that precede the cytokine secretion and accordingly used cells incubated for 2 h in increasing concentrations of NaCl for total lipid extraction and lipidome analysis by LC/MS. Quantified lipids were normalized to internal standards, added to the sample before lipid extraction and to total protein concentration.

The nontargeted lipidomic analysis identified 176 individual lipids, whereas another 274 potential lipid compounds remained unknown. Of the identified lipids, 108 lipid species (61.4%) showed significant positive or negative correlation (58 and 50 compounds, respectively) with the increase in NaCl concentration in the medium (Pearson correlation index above 0.5 or below 0.5). The lipid profile is presented as a heat map with fold changes in individual lipids in Fig. 2A.



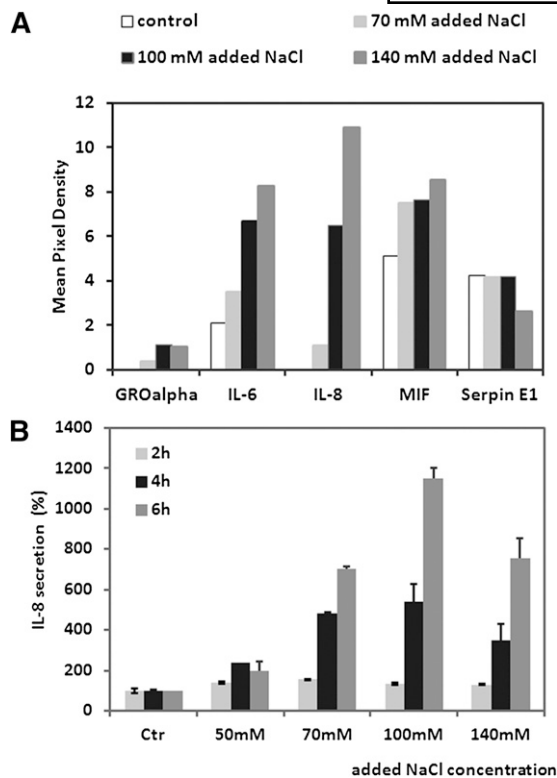


**Fig. 1.** Cytokine secretion from HCE2 cells after hyperosmolar stress. **A:** Cytokines modulated by HO-stress in HCE2 cells measured using a cytokine array kit. **B:** Time course of IL-8 secretion under HO stress. Error bars are mean  $\pm$  SEM from an average of three independent experiments as stated in the Material and Methods, Statistical analysis section.

Most affected lipid classes were the ceramides (Cers) and TGs with significant fold increases from nonstressed cells. Conversely, a few SM species and phosphatidylethanolamine (PE) levels were inversely correlated with the increase in extracellular osmolarity. Phosphatidylcholine species were not affected at this early phase of treatment (Fig. 2B).

When individual lipid species were evaluated in the Cer group, the most striking effect was observed for long-chain ceramides [Cer(d18:1/16:0), Cer(d18:1/18:0), and Cer(d18:1/21:1)] as shown in Fig. 2C. The intracellular accumulation of both Cer(d18:1/16:0) and Cer(d18:1/18:0) can be explained by the decrease in the corresponding SM species [exemplified in Fig. 2C inset for SM(d18:1/16:0)]. The increased TGs were very heterogeneous regarding the fatty-acyl chain length and number of double bonds, but dramatic fold increases were recorded, mainly for polyunsaturated TGs (Fig. 2D). Cholesterol levels, measured by an enzymatic method, were not significantly influenced by the HO stress (data not shown).

Considering the suggested correlation between ceramide accumulation and SM decrease, we measured sphingomyelinase activity in stimulated cells at neutral pH as well as under acidic conditions. After 1 h under HO conditions, the acid sphingomyelinase (ASM) remained unaffected, but activity at neutral pH increased with the ionic strength of the media. This effect was conserved at 2 h and

increased after 4 h. At this latter time point, NSM and ASM show significant activation in samples with high NaCl concentration ( $P < 0.05$ , as shown in Fig. 3A, B). Gene expression analysis of these samples highlighted NSM2 as the sphingomyelinase sensitive to HO (Fig. 3C). NSM2 transcription was progressively induced by NaCl up to 90 mM NaCl and then gradually decreased back to basal levels (Fig. 3D). Intriguingly, at these concentrations, where NSM2 expression seems to decline, the ASM enzyme shows increased enzymatic activity (Fig. 3B).

A deeper investigation into the sphingomyelin cycle revealed that 4 h after stress, stimulated cells displayed upregulated expression of neutral ceramidase, whereas its acidic counterpart remained unaffected (Fig. 3C, D). An elevated ceramidase activity suggests sphingosine (Sph) and, consequently, SIP production, inasmuch as Sph is highly toxic and its cellular accumulation must be avoided (26). Hence, we measured SIP production and secretion as well as expression of the SIP1-3 receptors (that we identified as being expressed by corneal epithelial cells in vivo; data not shown). Intracellular concentration of SIP remained relatively constant at 2 and 4 h after stimulation, but secretion decreased in cells stressed for 4 h (Fig. 3E). The absence of SIP extracellular signaling was strengthened by the observation that SIP1 receptor expression was upregulated under stress (Fig. 3C), because signaling through this receptor is followed by downregulation of its expression (27). The SM-cycle activation and the accumulation of Cer prompted us to assess the degree of cellular death as a result of the HO stimulation. After 2 h under stress conditions, more than 90% of the cells remained on the plate, whereas after 4 h, approximately 20% of the cells detached from the substrate. Significant cell death (more than 20%) was observed after 18 h in 140 mM of added NaCl solution (see supplementary Fig. 1).

TG accumulation measured by LC-MS/MS could be easily visualized in cells using Oil Red O staining and fluorescence microscopy (Fig. 4A–C) and estimated by Oil Red O isopropanol extraction as well (Fig. 4D). Enzymatic measurement of both total cholesterol and free cholesterol showed that the cells do not accumulate cholesterol and that the visualized lipid droplets are mostly composed of TGs (see supplementary Fig. II). Our first hypothesis was that these stress-induced LDs are active sites of lipolysis, and we therefore measured general TG lipolysis as well as mRNA levels for diglyceride acyltransferase 1 and 2 (DGAT1, 2) (as enzymes involved in TG synthesis), adipose tissue triglyceride lipase (ATGL), and hormone-sensitive lipase as enzymes involved in TG hydrolysis (Fig. 4E). The enzyme responsible for the TG synthesis in our cellular model was DGAT1, as demonstrated by specific knockdown with siRNA (Fig. 4G). DGAT1 gene silencing increased IL-8 secretion induced by low HO stress (70 mM of added NaCl; Fig. 4H), suggesting a protective role for LDs under low-stress conditions. DGAT2 silencing by siRNA transfection had no significant effect on lipid droplet formation or IL-8 secretion (see supplementary Fig. IIIA, B, respectively). The lipolysis assay suggested lipoprotein lipase (LPL) as an efficient lipolytic enzyme,

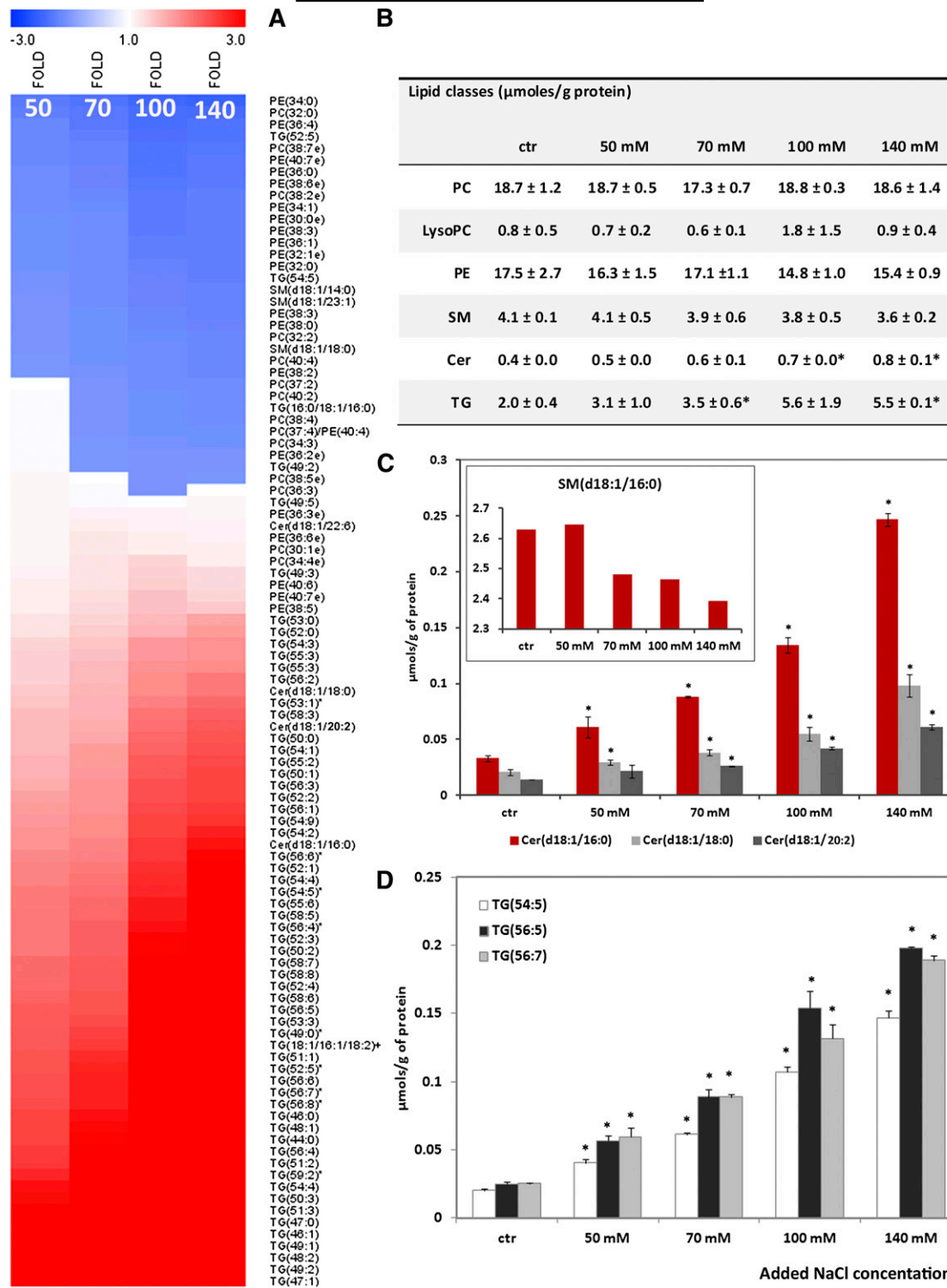


**Fig. 2.** Lipid profile of HO-stressed cells. **A:** Heat map of lipid species with fold changes in stimulated cells as compared with control. **B:** Quantification of specified lipid classes. **C:** Most stress-affected ceramide species; concurrent SM decrease is illustrated in the inset. **D:** TG accumulation exemplified by most-abundant TG species. \*  $P < 0.05$  as compared with control.

because TG hydrolysis measured in the absence of LPL stabilizers (heparin and apoC-II as LPL cofactors) was significantly lower. In both cases, lipolytic activity was attenuated by the addition of 90 mM NaCl (Fig. 4F). LPL, although an unlikely candidate for intracellular lipolysis, could contribute to the general lipolysis assay results,

because no releasing agent was used to remove LPL from the cell surface. Stressed cells did not differ from controls at transcriptional level, when genes involved in TG metabolism were analyzed (Fig. 4E; supplementary Table I).

Considering that the neutral lipids storage occurs in serum-deprived conditions, we searched for the FFA source

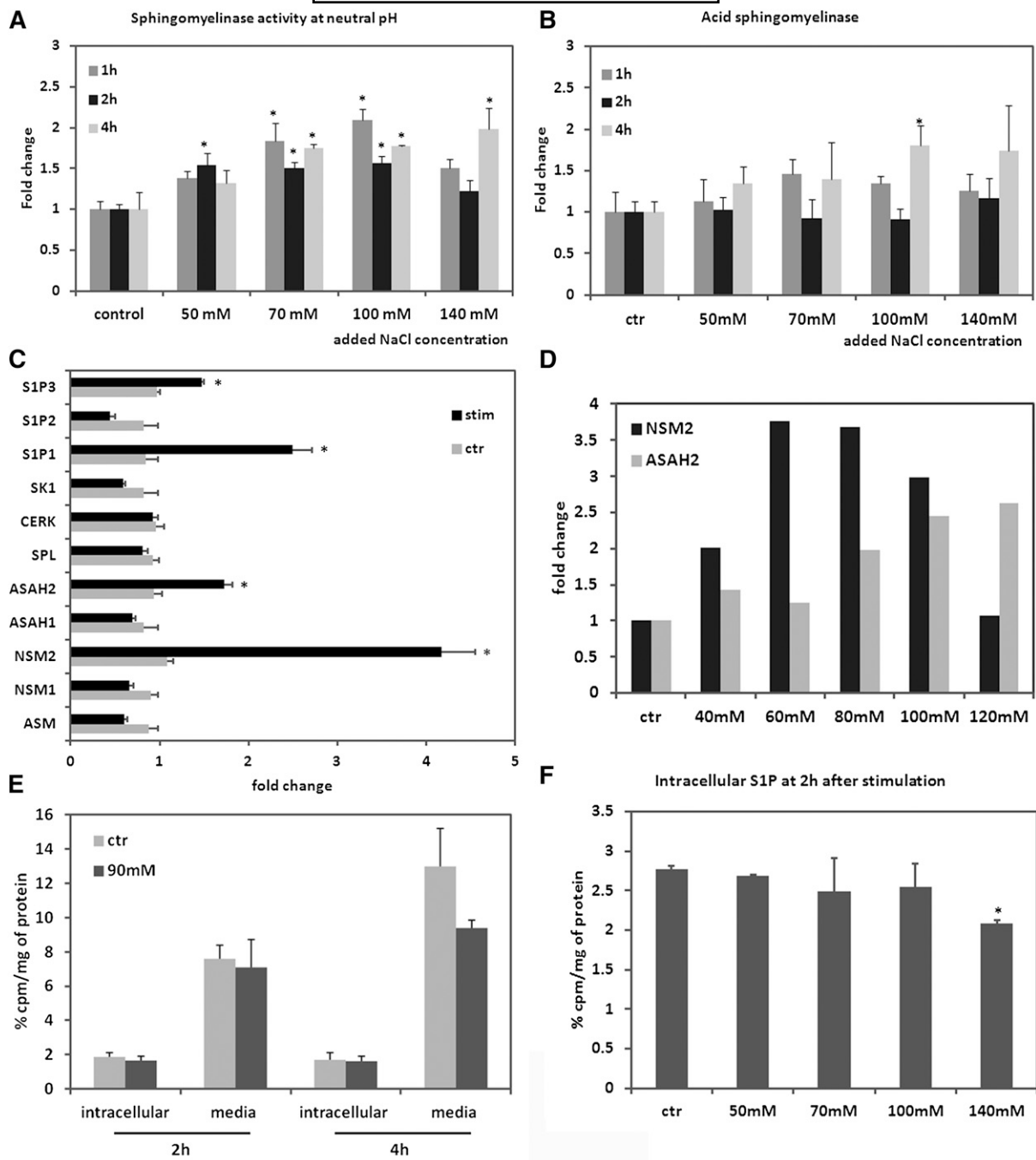


**Fig. 3.** Spingomyelin pathway activation in HO-stressed cells. A: Neutral sphingomyelinase activity. B: Acid sphingomyelinase activity. C: Gene expression data on SM pathway proteins. Cells were stimulated (black bars) with 90 mM of NaCl, and expression was measured after 4 h of incubation. D: NSM2, ASAH2 response to HO at mRNA level measured 4 h after stimulation. E: intracellular and secreted S1P in stressed cells versus control at 2 and 4 h after stimulation. F: Intracellular S1P production at 2 h after stimulation as a function of NaCl concentration in the medium. \*  $P < 0.05$  as compared with control.

that would induce TG synthesis. First, we investigated whether de novo synthesis was the source of FFAs to be used for TG formation. HCE cells were preincubated for 1 h with C75, a FAS inhibitor, after which HO was induced by adding NaCl to the media and TG droplets were quantified by the Oil Red O dye assay. FAS inhibition did not prevent the neutral lipid accumulation (Fig. 5A); however, this result was expected, because the measured effects of HO stress occur relatively quickly (1–2 h). Previous work

has suggested that the FFAs for stress-induced TG synthesis arise from phospholipid breakdown (16). S-bromo-enol lactone [(S)-BEL] efficiently prevented TG accumulation as well as IL-8 secretion (Fig. 5A, B), suggesting an involvement of the calcium-independent phospholipase A2 $\beta$  (iPLA2 $\beta$ ) in the events triggered by HO. iPLA2 $\beta$  was proven beforehand to be an enzyme involved in LD formation and, interestingly, as an upstream activator of sphingomyelinase (28, 29). Additionally, by blocking

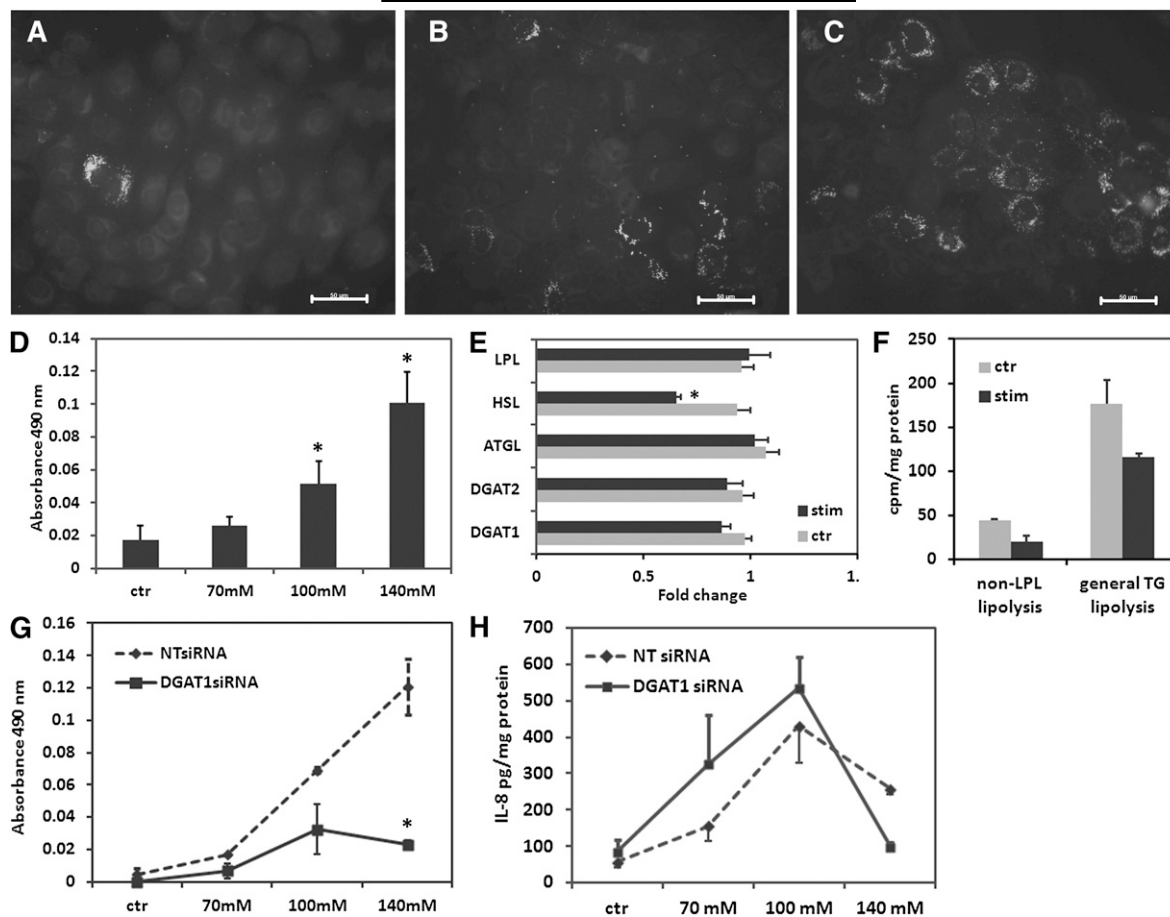


**Fig. 4.** Stress-induced lipid droplets in HCE2 cells. A–C: Oil Red O staining of cells stimulated with NaCl for 2 h: control, 70 mM and 100 mM, respectively. Images were acquired at  $\times 40$  magnification, and the scale bar represents 50  $\mu$ m. D: Oil Red O stain quantification using isopropanol extraction and colorimetric analysis at 490 nm. E: Expression data for genes involved in TG metabolism after 4 h under stress conditions. F: TG lipolysis in cells stimulated for 4 h versus control. G: LD formation under HO stress in DGAT1-silenced cells (DGAT1-siRNA) compared with cells transfected with the nontargeted siRNA (NTsiRNA). H: IL-8 secretion from stressed HCE cells after DGAT1 knockdown. \*  $P < 0.05$  as compared with control.

clathrin-dependent endocytosis with chlorpromazine, TG synthesis was obstructed to the same extent as with (S)-BEL (see supplementary Fig. 4A). IL-8 secretion, on the other hand was stimulated in the presence of the endocytosis inhibitor (see supplementary Fig. 4B).

Consequently, we investigated a possible link between sphingomyelinase-mediated ceramide production and LD development. To reliably impede ceramide production, we silenced the NSM2 gene using siRNA transfection. The interfering RNA blocked NSM2 upregulation upon HO stimulation and also significantly decreased IL-8 secretion from the HCE cells (Fig. 5E, D, respectively). Figure 5E also shows that BEL treatment impeded NSM2 gene upregulation under HO conditions. Cellular TG accumulation was significantly reduced, as verified by Oil Red O isopropanol extraction (Fig. 5C). Knock-down efficiency is presented at mRNA level as well as enzymatic activity at neutral pH in Fig. 5G, H, respectively.

In mammalian cells, p38 MAPK is the HO stress response kinase (30), and previous studies have linked the activity of this kinase to sphingolipid signaling (31, 32).

We employed the SB239063 inhibitor to test the involvement of the p38 MAPK in our experimental setup and found that it strongly inhibited IL-8 secretion upon stress, but did not affect TG droplet formation (Fig. 5A, B).

## DISCUSSION

The surface of the eye is in constant contact with the external environment and hence subjected to numerous aggressions. HO is a clinically relevant stress factor for the corneal epithelium, and this condition is a consequence of either increased evaporation, decreased production of tears, or changes in the composition of the tear fluid (33). HO is accompanied both in vivo and in vitro by a proinflammatory response, and we have used IL-8 secretion from HCE2 cells as an inflammatory marker in our experimental design.

HO causes an undeniable stress on membranes, and our aim was to reveal how lipid homeostasis is affected by this extracellular stimulus. We have employed a lipidomic approach that brought forward ceramides and TGs as altered lipid classes. Here, we show that high osmolarity induces cellular TG build-up as LDs and that furthermore,



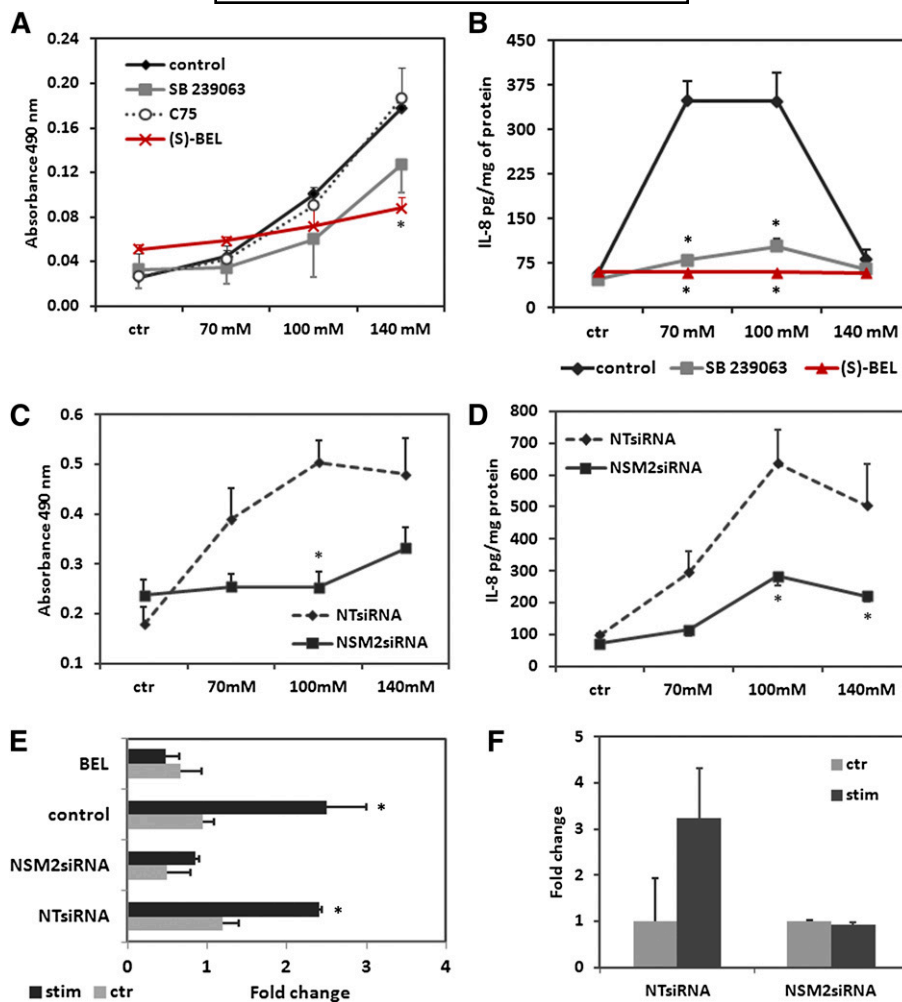


**Fig. 5.** NSM2 regulates HO-induced LD formation. A: Oil Red O stain quantification of HO stress-induced TG accumulation after inhibition of FAS (10  $\mu$ g/ml C75), iPLA2 (10  $\mu$ M (S)-BEL) or p38 MAPK (10  $\mu$ M SB 239063). B: IL-8 secretion in cells incubated with SB 239063 (10  $\mu$ M) and (S)-BEL (10  $\mu$ M) compared with control. C: LD quantification in NSM2-silenced cells (NSM2siRNA) compared with cells transfected with control siRNA (NTsiRNA). D: IL-8 levels in media from NSM2 siRNA-transfected cells. E: NSM2 siRNA transfection efficiency measured at mRNA levels in stimulated and nonstimulated cells and BEL effect on NSM2 gene transcription under basal or stimulated conditions. F: Neutral sphingomyelinase activity in cells transfected with NTsiRNA compared with NSM2-silenced cells. In the experiments involving inhibitors, cells were preincubated for 1 h in the presence of the inhibitor alone followed by osmolar stress induction with NaCl. \*  $P < 0.05$  as compared with control.

this process is closely coupled to ceramide production through NSM2 activity.

Although ASM and NSMs are known as stress response enzymes, this is, to our knowledge, the first time that the NSM2 is reported to respond to osmolarity variations. The stress-dependent increase in ceramides proved to be a reliable indicator of the SM pathway activation by HO. We investigated SM hydrolysis as the source of ceramides because of the apparent, although not statistically significant, corresponding decrease in SM species. This trend was most evident for the Cer(d18:1/16:0)-SM(d18:1/16:0) pair. Similar trends were more difficult to observe for other Cer species if we consider the disproportionality between the lipid species, inasmuch as the highest Cer concentration measured was 10-fold lower than the level of the corresponding SM. We tested for enzymatic activation

starting 5 min after the addition of the stimulus (data not shown), but we could measure a significant response in sphingomyelinase activity only after 1 h under HO stress conditions, suggesting that SM pathway activation might be an effector more than a sensor of HO-induced membrane stress. Moreover, we observed an almost-linear induction of enzymatic activity with stress that was reflected at gene expression level as well. NSM2 gene transcription was linearly induced by the addition of less than 90 mM of NaCl, after which it gradually returned to basal levels. Conversely, ASA2 transcription was induced by the higher sodium concentrations (>80 mM NaCl).

Considering the regulation and crucial balance in sphingolipid metabolism, information on one compound does not provide a comprehensive representation of cellular response status. Gene expression analysis after 4 h suggested




upregulated ceramidase activity, which could defuse the harmful accumulation of proapoptotic ceramides. However, at the osmotic pressure at which both sphingomyelinase and ceramidase expression peaked, intracellular SIP production decreased. This implies that SM hydrolysis to ceramide is not counterbalanced by production of the prosurvival metabolite SIP. An increased SIP lyase activity in stimulated cells that would irreversibly eliminate the sphingolipid could be an alternative, but we found no evidence of this in the gene expression analysis.

Lipidomic analysis revealed that in addition to ceramide accumulation, HO induces LD formation, seen as a linear intracellular build-up of TGs with the added NaCl. This process was independent of de novo synthesis of FFAs, but was very sensitive to BEL treatment and seemingly independent of cyclooxygenase activity. Moreover, BEL prevented NSM2 gene upregulation in response to HO. The suggested iPLA2 $\beta$  role is defended to some extent in our model by the decrease in PE species measured in the lipidomic analysis and by the inhibitory effect of endocytosis blockage on the TG build-up. PLA2 enzymes are not novel candidates for stress-associated LD biogenesis, and iPLA2 was recently linked to high-salt response in *Chlamydomonas* (28, 34). LD biogenesis in various types of cellular stress has become a very active field of research during recent years, and it is presently considered a generalized response (16). This response could be an efficient way to suppress lipotoxicity induced by FFA production resulting from PLA2 activation, thus increasing cell viability under stress (15). NSM2 knock-down had effects comparable to BEL treatment in lowering both cytokine secretion and formation of TG-enriched droplets and tightly linked ceramide production to both major outcomes. The delayed NSM2 response to HO stress suggests that SM pathway activation is a downstream event in the HO-induced pathway; however, the molecular sensors for high osmolarity remain to be identified. Phospholipase activity together with the ceramide production might be events targeted at eliminating the pressure imposed on the plasma membrane by the cell shrinkage in the HO environment. This membrane stress is then eliminated by stimulated endocytosis of the “extra” membrane, and phospholipids are then recycled as stress droplets.

The HO-responsive p38 MAPK is a known activator of NSM2 (30), but surprisingly, its inhibition had no effect on LD formation, affecting only the proinflammatory outcome of the stress. This finding proposes a downstream position for p38 from NSM2 in our experimental set-up, as other studies have previously suggested (35).

HO stress is an environmental hazard with important effects on the ocular surface, and a well-concerted cellular response becomes a defining factor between healthy and dysfunctional cornea. This is clinically translated into DES, the most-common inflammatory disease of the cornea. We have shown here that NSM2 blockage inhibits almost completely IL-8 chemokine secretion from HCE2 cells. The same effect was observed after BEL and p38 MAPK inhibitor treatment. This anti-inflammatory effect would at least minimize the pathological outcome associated with the

stress condition by reducing immune cell recruitment as well as the “outside in” effects of IL-8 signaling. Induction of the HO-stress pathway causes complex responses in cells; therefore, identification of participants and branching points is needed in order to start any therapeutic approaches. Hyperosmolar tear fluid has been associated with decreased cell viability and delayed wound healing (36); hence, an efficient DES treatment should aim at restoring tissue homeostasis and at not inducing additional metabolic turbulence.

Nontargeted lipidomic analysis proved to be an important tool, inasmuch as it provided a hypothesis-free approach to this study, eliminating biased search for possible activated pathways. Data analysis revealed that HO stress in epithelial cells is accompanied by significant rearrangements in cell lipidomes and small-scale changes in abundant lipids can translate to large-scale changes in rare lipid classes, such as Cers and TGs. In our experimental model, we showed an important participation of NSM2 in the cellular stress response to increased osmolarity. LD formation is not an event relevant only for our cellular model, but could have implications in other systems as well. Schwartz et al. (37) revealed that pathogen-related inflammatory reaction increases the osmolarity of inflammatory fluids. Given that inflammation is an essential cellular response to all stress inducers, its intimate connection with HO becomes an important issue in contexts different from that of the corneal surface or DES. Thus, revealing the details of this signaling pathway is an important near-future target of our research. 

The authors thank Jari Metso for valuable technical help.

## REFERENCES

1. Hallows, K. R., F. Y. Law, C. H. Packman, and P. A. Knauf. 1996. Changes in cytoskeletal actin content, F-actin distribution, and surface morphology during HL-60 cell volume regulation. *J. Cell. Physiol.* **167**: 60–71.
2. Tomlinson, A., S. Khanal, K. Ramaesh, C. Diaper, and A. McFadyen. 2006. Tear film osmolarity: determination of a referent for dry eye diagnosis. *Invest. Ophthalmol. Vis. Sci.* **47**: 4309–4315.
3. Pflugfelder, S. C., S. C. Tseng, O. Sanabria, H. Kell, C. G. Garcia, C. Felix, W. Feuer, and B. L. Reis. 1998. Evaluation of subjective assessments and objective diagnostic tests for diagnosing tear-film disorders known to cause ocular irritation. *Cornea.* **17**: 38–56.
4. Magnoni, C., E. Euclidi, L. Benassi, G. Bertazzoni, A. Cossarizza, S. Seidenari, and A. Giannetti. 2002. Ultraviolet B radiation induces activation of neutral and acidic sphingomyelinases and ceramide generation in cultured normal human keratinocytes. *Toxicol. In Vitro.* **16**: 349–355.
5. Grassmé, H., E. Gulbins, B. Brenner, K. Ferlinz, K. Sandhoff, K. Harzer, F. Lang, and T. F. Meyer. 1997. Acidic sphingomyelinase mediates entry of *N. gonorrhoeae* into nonphagocytic cells. *Cell.* **91**: 605–615.
6. Colombaroni, L., L. M. Frago, I. Varela-Nieto, R. Pesí, and M. Garcia-Gil. 2002. Serum deprivation increases ceramide levels and induces apoptosis in undifferentiated HN9.10e cells. *Neurochem. Int.* **40**: 327–336.
7. Cuvillier, O., G. Pirianov, B. Kleuser, P. G. Vanek, O. A. Coso, S. Gutkind, and S. Spiegel. 1996. Suppression of ceramide-mediated programmed cell death by sphingosine-1-phosphate. *Nature.* **381**: 800–803.
8. Yang, L., Y. Ding, Y. Chen, S. Zhang, C. Huo, Y. Wang, J. Yu, P. Zhang, H. Na, H. Zhang, et al. 2012. The proteomics of lipid

- droplets: structure, dynamics, and functions of the organelle conserved from bacteria to humans. *J. Lipid Res.* **53**: 1245–1253.
9. Sturley, S. L., and M. M. Hussain. 2012. Lipid droplet formation on opposing sides of the endoplasmic reticulum. *J. Lipid Res.* **53**: 1800–1810.
  10. Murphy, D. J. 2001. The biogenesis and functions of lipid bodies in animals, plants and microorganisms. *Prog. Lipid Res.* **40**: 325–438.
  11. Quintero, M., M. E. Cabanas, and C. Arus. 2007. A possible cellular explanation for the NMR-visible mobile lipid (ML) changes in cultured C6 glioma cells with growth. *Biochim. Biophys. Acta.* **1771**: 31–44.
  12. Iorio, E., M. Di Vito, F. Spadaro, C. Ramoni, E. Lococo, R. Carnevale, L. Lenti, R. Strom, and F. Podo. 2003. Triacsin C inhibits the formation of 1H NMR-visible mobile lipids and lipid bodies in HuT 78 apoptotic cells. *Biochim. Biophys. Acta.* **1634**: 1–14.
  13. Bozza, P. T., J. L. Payne, S. G. Morham, R. Langenbach, O. Smithies, and P. F. Weller. 1996. Leukocyte lipid body formation and eicosanoid generation: cyclooxygenase-independent inhibition by aspirin. *Proc. Natl. Acad. Sci. USA.* **93**: 11091–11096.
  14. Dvorak, A. M., P. F. Weller, V. S. Harvey, E. S. Morgan, and H. F. Dvorak. 1993. Ultrastructural localization of prostaglandin endoperoxide synthase (cyclooxygenase) to isolated, purified fractions of guinea pig peritoneal macrophage and line 10 hepatocarcinoma cell lipid bodies. *Int. Arch. Allergy Immunol.* **101**: 136–142.
  15. Du, L., R. W. Hickey, H. Bayir, S. C. Watkins, V. A. Tyurin, F. Guo, P. M. Kochanek, L. W. Jenkins, J. Ren, G. Gibson, et al. 2009. Starving neurons show sex difference in autophagy. *J. Biol. Chem.* **284**: 2383–2396.
  16. Gubern, A., M. Barcelo-Torns, J. Casas, D. Barneda, R. Masgrau, F. Picatoste, J. Balsinde, M. A. Balboa, and E. Claro. 2009. Lipid droplet biogenesis induced by stress involves triacylglycerol synthesis that depends on group VIA phospholipase A2. *J. Biol. Chem.* **284**: 5697–5708.
  17. Araki-Sasaki, K., Y. Ohashi, T. Sasabe, K. Hayashi, H. Watanabe, Y. Tano, and H. Handa. 1995. An SV40-immortalized human corneal epithelial cell line and its characterization. *Invest. Ophthalmol. Vis. Sci.* **36**: 614–621.
  18. Blish, E. G., and W. J. Dyer. 1959. A rapid method of total lipid extraction and purification. *Can. J. Biochem. Physiol.* **37**: 911–917.
  19. Nygren, H., T. Seppanen-Laakso, S. Castillo, T. Hyotylainen, and M. Oresic. 2011. Liquid chromatography-mass spectrometry (LC-MS)-based lipidomics for studies of body fluids and tissues. *Methods Mol. Biol.* **708**: 247–257.
  20. Pluskal, T., S. Castillo, A. Villar-Briones, and M. Oresic. 2010. MZmine 2: modular framework for processing, visualizing, and analyzing mass spectrometry-based molecular profile data. *BMC Bioinformatics.* **11**: 395.
  21. Mitra, P., S. G. Payne, S. Milstien, and S. Spiegel. 2007. A rapid and sensitive method to measure secretion of sphingosine-1-phosphate. *Methods Enzymol.* **434**: 257–264.
  22. Ehnholm, C., and T. Kuusi. 1986. Preparation, characterization, and measurement of hepatic lipase. *Methods Enzymol.* **129**: 716–738.
  23. Németh, Z. H., E. A. Deitch, C. Szabo, and G. Hasko. 2002. Hyperosmotic stress induces nuclear factor-kappaB activation and interleukin-8 production in human intestinal epithelial cells. *Am. J. Pathol.* **161**: 987–996.
  24. Massingale, M. L., X. Li, M. Vallabhajosyula, D. Chen, Y. Wei, and P. A. Asbell. 2009. Analysis of inflammatory cytokines in the tears of dry eye patients. *Cornea.* **28**: 1023–1027.
  25. Spandau, U. H., A. Toksoy, S. Verhaart, R. Gillitzer, and F. E. Kruse. 2003. High expression of chemokines Gro-alpha (CXCL-1), IL-8 (CXCL-8), and MCP-1 (CCL-2) in inflamed human corneas in vivo. *Arch. Ophthalmol.* **121**: 825–831.
  26. Contreras, F. X., J. Sot, A. Alonso, and F. M. Goni. 2006. Sphingosine increases the permeability of model and cell membranes. *Biophys. J.* **90**: 4085–4092.
  27. Schwab, S. R., and J. G. Cyster. 2007. Finding a way out: lymphocyte egress from lymphoid organs. *Nat. Immunol.* **8**: 1295–1301.
  28. Gubern, A., J. Casas, M. Barcelo-Torns, D. Barneda, X. de la Rosa, R. Masgrau, F. Picatoste, J. Balsinde, M. A. Balboa, and E. Claro. 2008. Group IVA phospholipase A2 is necessary for the biogenesis of lipid droplets. *J. Biol. Chem.* **283**: 27369–27382.
  29. Lei, X., S. Zhang, S. E. Barbour, A. Bohrer, E. L. Ford, A. Koizumi, F. R. Papa, and S. Ramanadham. 2010. Spontaneous development of endoplasmic reticulum stress that can lead to diabetes mellitus is associated with higher calcium-independent phospholipase A2 expression: a role for regulation by SREBP-1. *J. Biol. Chem.* **285**: 6693–6705.
  30. Han, J., J. D. Lee, L. Bibbs, and R. J. Ulevitch. 1994. A MAP kinase targeted by endotoxin and hyperosmolarity in mammalian cells. *Science.* **265**: 808–811.
  31. Clarke, C. J., T. G. Truong, and Y. A. Hannun. 2007. Role for neutral sphingomyelinase-2 in tumor necrosis factor alpha-stimulated expression of vascular cell adhesion molecule-1 (VCAM) and intercellular adhesion molecule-1 (ICAM) in lung epithelial cells: p38 MAPK is an upstream regulator of nSMase2. *J. Biol. Chem.* **282**: 1384–1396.
  32. Filosto, S., W. Fry, A. A. Knowlton, and T. Goldkorn. 2010. Neutral sphingomyelinase 2 (nSMase2) is a phosphoprotein regulated by calcineurin (PP2B). *J. Biol. Chem.* **285**: 10213–10222.
  33. Definition and Classification Subcommittee of the International Dry Eye WorkShop. 2007. The definition and classification of dry eye disease: report of the Definition and Classification Subcommittee of the International Dry Eye WorkShop. *Ocul. Surf.* **5**: 75–92.
  34. Arisz, S. A., and T. Munnik. 2011. The salt stress-induced LPA response in *Chlamydomonas* is produced via PLA2 hydrolysis of DGK-generated phosphatidic acid. *J. Lipid Res.* **52**: 2012–2020.
  35. Mondal, S., C. Mandal, R. Sangwan, and S. Chandra. 2010. Withanolide D induces apoptosis in leukemia by targeting the activation of neutral sphingomyelinase-ceramide cascade mediated by synergistic activation of c-Jun N-terminal kinase and p38 mitogen-activated protein kinase. *Mol. Cancer.* **9**: 239.
  36. Epidemiology Subcommittee of the International Dry Eye WorkShop. 2007. The epidemiology of dry eye disease: report of the Epidemiology Subcommittee of the International Dry Eye WorkShop. *Ocul. Surf.* **5**: 93–107.
  37. Schwartz, L., A. Guais, M. Pooya, and M. Abolhassani. 2009. Is inflammation a consequence of extracellular hyperosmolarity? *J. Inflamm. (Lond.)* **6**: 21.